Spin-affected droplet coalescence and separation undergoing off-center collision

Chengming He[1,2], Jun Hu[3], Lianjie Yue[1,2], Peng Zhang*[4]
[1]Lab of Aerospace Science and Technology, Institute of Mechanics, Chinese Academy of Sciences, Beijing, China
[2]State Key Laboratory of High Temperature Gas Dynamics, Institute of Mechanics, Chinese Academy of Sciences, Beijing, China
[3]Institute of Applied Physics and Computational Mathematics, Beijing, China
[4]Department of Mechanical Engineering, The Hong Kong Polytechnic University, Hong Kong
*Corresponding author email: pengzhang.zhang@polyu.edu.hk

Abstract
A recent study (Phys. Review Fluids 5, 113601, 2020) has demonstrated the importance of initial droplet spin on their bouncing, coalescence, and separation for a specific case upon head-on collision. In this paper, a computational study by using the Volume-of-Fluid (VOF) method was performed to investigate the spin-affected coalescence-separation transition for more practical situations of off-center collision. First, a parametric study on droplet separation modes with varying spinning speed (ω_0) and impact parameter (B) was analysed, showing that droplet spin influences reflexive and stretching separations with different mechanisms. Second, the influence of spin chirality on coalescence-separation boundary transition was studied. A prominent finding is that the spin angular momentum of the merged droplet accounts for the droplet separation, in which increasing spin angular momentum by a droplet spin suppress reflective separation while promote stretching separation, and decreasing spin angular momentum by a opposite droplet spin negligibly influence reflexive separation while suppress stretching separation.

Keywords
Droplet spin; Separation; Ligament breakup; Spin chirality; VOF simulation;

I. Introduction

Collision between two droplets in a gaseous environment is of relevance to many natural and industrial processes, which has been reviewed[1, 2] in the literature. Generally, two colliding droplets tend to merge into a united droplet with small impacting velocity and temporary coalescence followed by separation with generating satellite droplets if the inertia force exceeds the surface tension force[3-5]. The number and size of satellite droplets are significant to the fuel atomization in the spray combustion engines[6].

Most of experimental studies[3, 5, 7-11] identified and interpreted various outcomes, such as coalescence, bouncing, and separation by a well-known collision nomogram in the We-B parameter space, as the schematic shown in Fig. 1. The collision Weber number, We, which measures the relative importance of the droplet inertia compared to the surface tension, and the impact parameter, B, which measures the deviation of the trajectory of droplets from that of the head-on collision, with B=0 denoting the head-on collision and B=1 the grazing collision. The present study was focused on the transition region between coalescence and separation (either reflexive or stretching separation) only, that denoted by the red lines in Fig. 1. For We of the order O(10^2), as increasing B, droplet collision outcomes show a non-monotonic variation from reflexive separation to coalescence and to stretching separation. In addition, the influences of some other controlling parameters on the boundaries have also been

investigated, such as the droplet Ohnesorge number[7, 9], Oh, which measures the relative importance of the liquid viscous stress compared to the capillary pressure, and the size ratio[3, 11, 12], Δ, which measures the droplet size disparity. As increasing Oh and Δ, the boundaries between coalescence and separation regime move towards a larger We, owing to the enhanced viscous dissipation.

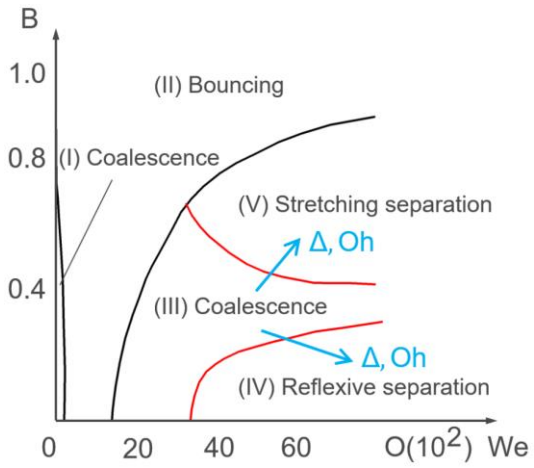

Figure 1. Schematic of the collision nomogram in the We-B parameter space.

The models and mechanisms describing droplet coalescence and separation have been reported by extensively studies[3-5, 8, 10-12]. For the specific case of head-on collision[5, 10], reflexive separation, i.e. in regime IV, occurs if the inertia force of the rebounding motion is larger than the surface tension force, or via an evaluation of the kinetic energy against the surface energy. It is similar for collisions at small B, since the entire process shows flattening and elongation followed by separation is nearly head-on. For collisions at sufficient large B, stretching mechanics was claimed to account for the stretching separation without large droplet deformation[3, 5], by considering the stretching inertia force against the surface tension force and viscous force. Furthermore, for collisions at intermediate B and large We, a new regime named “rotational separation” were introduced[13] that located in the coalescence regime, whose the criterion is interpreted by balancing surface tension force and angular momentum[4, 5] or via an evaluation of the rotational energy against surface energy, because previous experimental[3, 5] and numerical[14-17] studies have demonstrated that the merged droplet can spin after off-center collisions.

It is worthy to noted that in practical situations the droplet collision is more complicated than the case discussed above. The spinning motion can be created either from droplet injectors (by nonuniform driving pressure or uneven injector surface) or from preceding collisions. In particular, the off-center collision-induced spinning droplets can collide with each other because subsequent collisions are highly probable in practical dense sprays[18, 19]. In recent study, He and Zhang[17] studied the head-on bouncing and found the spinning droplet can induce significant non-axisymmetric droplet deformation because of the conversion of the spin angular momentum into the orbital angular momentum. Further, they also studied the head-on coalescence between a spinning droplet and a non-spinning droplet of equal size and found the spinning motion can promote the mass interminglement of droplets because the locally nonuniform mass exchange occurs at the early collision stage by non-axisymmetric flow and is further stretched along the filament at later collision stages. Apart from the study of spinning

effects on droplet bouncing and coalescence, the spin-affected droplet separation and subsequent satellite droplet formation are highly probable in practical dense sprays, but relevant studies have not been reported in the literature.

Thus, in this paper, we shall present a computational study on the coalescence-separation transition for collisions between spinning droplets. The presentation of the study is organized as follows. The numerical methodology and specifications are described in Sec. II. The results of the separation modes influenced by the impact parameter and droplet spinning speed are presented in Sec. III, followed by the influences of spin chirality in Sec. IV.

II. Numerical methodology and specifications

A. Methodology and validations

The three-dimensional continuity and incompressible Navier-Stokes equations,

$$\nabla\cdot\boldsymbol{u}=0 \tag{1}$$

$$\rho(\partial\boldsymbol{u}/\partial t+\boldsymbol{u}\cdot\nabla\boldsymbol{u})=-\nabla p+\nabla\cdot(2\mu\boldsymbol{D})+\sigma\kappa\boldsymbol{n}\delta_s \tag{2}$$

are solved by using the classic fractional-step projection method, where $\boldsymbol{u}$ is the velocity vector, ρ the density, p the pressure, μ the dynamic viscosity, and $\boldsymbol{D}$ the deformation tensor defined as $D_{ij}=(\partial_j u_i+\partial_i u_j)/2$. In the surface tension term $\sigma\kappa\boldsymbol{n}\delta_s$, δ_s is a Dirac delta function, σ the surface tension coefficient, κ the local curvature, and the unit vector $\boldsymbol{n}$ normal to the local interface.

To solve both the gas and liquid phases, the density and viscosity are constructed by the volume fraction as $\rho=c\rho_l+(1-c)\rho_g$ and $\mu=c\mu_l+(1-c)\mu_g$, in which the subscripts l and g denote the liquid and gas phases, respectively. The volume fraction c satisfies the advection equation

$$\partial c/\partial t+\nabla\cdot(c\mathbf{u})=0 \tag{3}$$

with $c=1$ for the liquid phase, $c=0$ for the gas phase, and $0<c<1$ for the gas-liquid interface. The present study adopts the Volume-of-Fluid (VOF) method, which has been implemented in the open source code, Gerris[20], featuring the three-dimensional octree adaptive mesh refinement, the geometrical VOF interface reconstruction, and continuum surface force with height function curvature estimation. Gerris has been demonstrated to be competent for high-fidelity simulation of a wide range of multiphase flow problems[14-17, 21-24].

A major challenge of VOF simulations on droplet collision lies in the inability of the Navier-Stokes equations in describing the rarified gas effects and the Van der Waals force[25] within the gas film, thereby prohibiting the physically correct prediction of droplet coalescence. A coarse mesh would induce “premature” coalescence of the droplets that realistically bounce off. Thus, the successful simulation of droplet coalescence and subsequent collision dynamics in previous studies[17, 22] were obtained by choosing an appropriate mesh resolution near the interface. It is worthy to mention that mesh dependence is not a significant issue for the simulation of droplet coalescence followed by separation in the present study because the drainage of gas film occurs shortly upon the droplet collision at large We.

To improve computational efficiency, different mesh refinement level (N_g,N_l,N_i) is used in three physical zones, namely the gas, the droplet, and the interface zones, that divided from the entire computational domain. As a balance between computational cost and accuracy, a mesh refinement level of (4, 7, 8) was used[17] for all simulations in the present study. It takes about 200 hours of real time to run the simulation up to T=2.0 on two Intel Xeon(R) Gold-6150 processor with 72 cores (36 cores for each processor). The numerical validations against

experiments and grid independence analysis of droplet coalescence were conducted in detail in our previous studies[17] and will not be repeated in the present paper.

B. Problem description and numerical specifications

The 3D computational domain of the droplet collision is illustrated in Fig. 2. Two droplets of diameter D are specified to collide along the x-direction with a relative translational velocity, U, and therefore they have zero relatively velocities in the y- and z- directions. Without losing generality, the translational velocity component for droplet O_1 and O_2 are set as $-\frac{U}{2}$ and $\frac{U}{2}$ along the x-direction, respectively, so that the linear momentum of the entire mass-center system remains zero. For off-center collisions, the deviation of the mass centers from the head-on collision is qualified by χ, which is defined as the projection of the connection line O_1O_2 (hereinafter referred to $\overline{O_1O_2}$) along the z-direction. The spin axis l_{O_1} can be described by a polar angle θ with respect to the z-axis and an azimuthal angle φ to the x-axis. In the present study, the polar angle θ is fixed at $\pi/2$ and the azimuthal angle varies in the range of $0 \le \varphi \le \pi/2$. As a result, the initial spin angular velocity can be expressed as $\boldsymbol{\omega_0=(-\omega_0 cos\varphi, -\omega_0 sin\varphi, 0)}$, and the spinning velocity components of droplet O_1 is given by $H(c_1\text{-}1)\boldsymbol{\omega_0 \times (r-R_{O_1})}$, where the Heaviside step function ensures the assignment of spin to droplet O_1 only. The domain is $6D$ in length and $4D$ in both width and height; all the boundaries are specified with the free outflow boundary conditions.

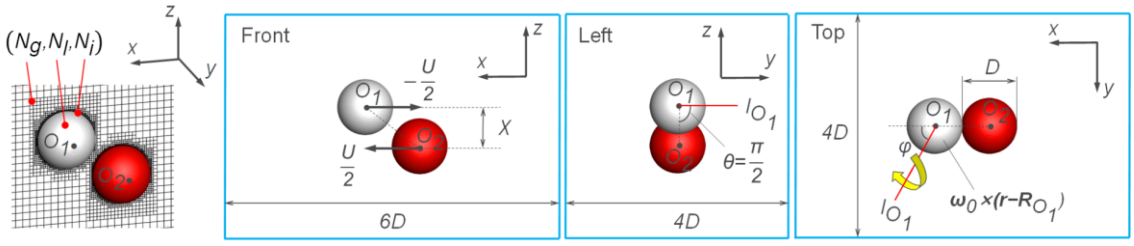

Figure 2. Computational setup of a off-center collision between a spinning droplet 1 and a non-spinning droplet 2.

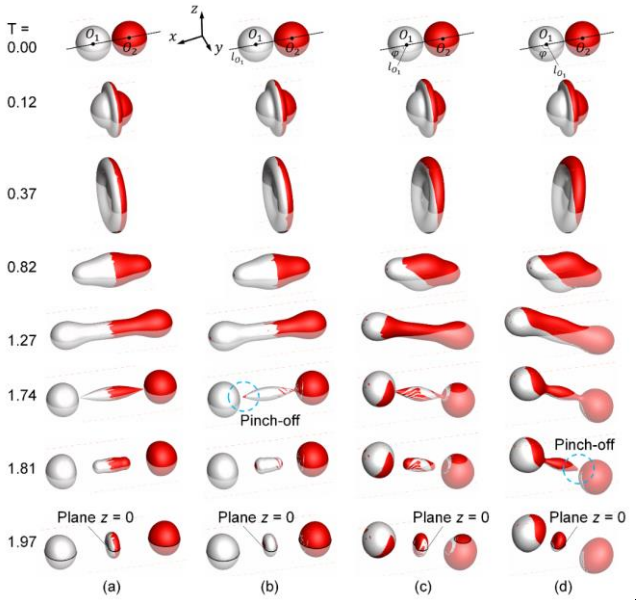

Figure 3. Evolution of droplet deformation upon a head-on collision at We=61.4, $Oh=2.8\times10^{-2}$ and ω_0=3 with varying azimuthal angle of droplet O_1. (a) non-spinning, (b) φ=0, (c) $\varphi=\pi/4$, and (d) $\varphi=\pi/2$.

As shown in Fig. 3, the deformation of the head-on collision between two non-spinning droplets in Fig. 3(a) is axisymmetric by x-axis and mirror symmetry by the y-z plane. Whereas for collisions between spinning droplets, as shown in Fig. 3(b-d) with varying φ, the axisymmetric droplet deformation is deviated from the head-on collision and the mirror symmetry are broken owing to the spinning motion of droplet O_1, and droplet separation followed by the pinch-off of the ligament is delayed when compared to that in Fig. 3(a) because of the enhanced viscous dissipation. The interaction between the spinning motion of O_1 and the translational motion of two droplets is strongest[17] at $\varphi=\pi/2$. To simply the parametric study, the azimuthal angle φ is fixed at $\pi/2$, although the post-collision velocities of the separated droplets are of significant relevance to the spinning axis that merits future studies. In addition, to further simply the problem but not lose generality, this study restricts its scope to the collision between two equal-sized droplets (Δ=1.0) with fixed $Oh=2.8\times10^{-2}$ so as to avoid unnecessary complexity of geometrical asymmetry and size disparity. Consequently, the present numerical study focuses on the controlling parameters in the range of We=40~85, B=0~1 and ω_0=0~6.

III. Separation modes influenced by ω_0 and B

Figure 4 shows droplet separation modes that influenced by the impact parameter B and the droplet spinning speed ω_0. For collisions at small B, e.g. the head-on collision at B=0.0, the reflexive separation is suppressed as increasing ω_0, which is attributed to the enhanced viscous dissipation[17] induced by the interaction between the spinning motion and translational motion of droplets. For collisions at intermediate B, e.g. the off-center collision at B=0.4, the stretching separation is promoted as increasing ω_0, because the initial spinning motion increases the spin angular momentum of the united droplet so as to exceed the surface tension force and lead to the droplet separation. For collisions at sufficient large B, e.g. the nearly grazing collision at B=0.9, as increasing ω_0, the spinning motion lead to a longer ligament and then breakup into more satellite droplets. This is because the stretching effects is enhanced by the droplet spin.

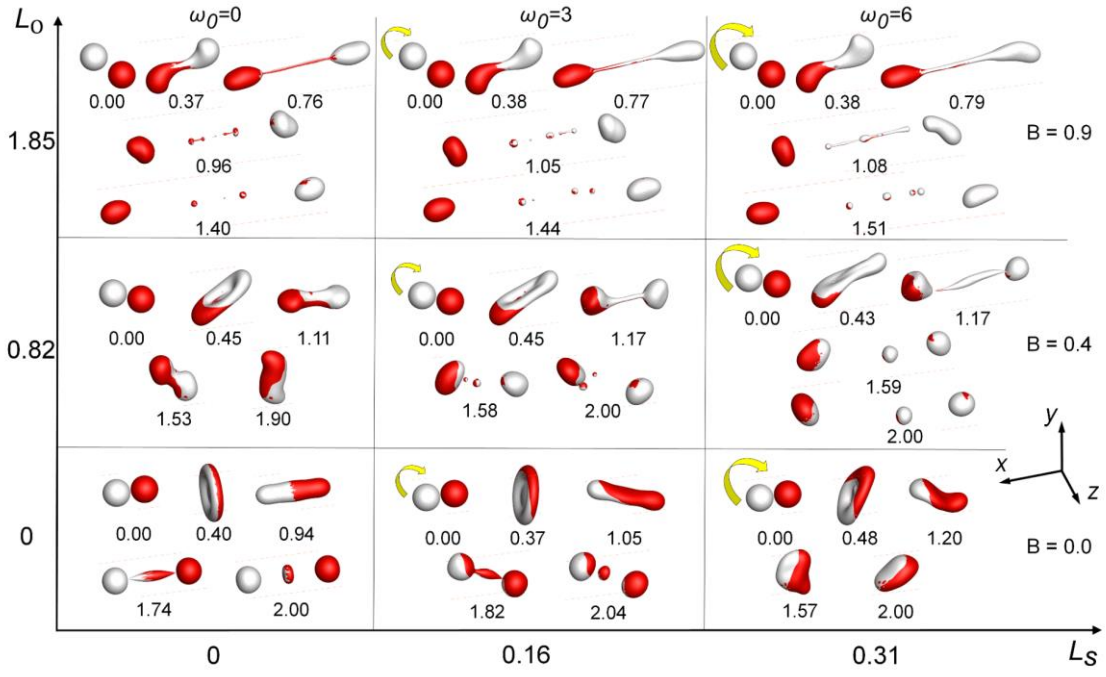

Figure 4. Numerical results of the separation modes between a spinning droplet (left) and a non-spinning droplet (right) with varying spinning speed ω_0 and impact parameter B at fixed We=61.4 and Oh=2.8×10^{-2}.

To further analyse the separation mechanism for collisions at intermediate and large *B*, Figure 5 shows the contour of vorticity in the y-direction that reflecting the local spinning motion during droplet deformation. It is seen that the vorticity transport is point symmetry based on the origin in Fig 5(a) for collision between two non-spinning droplets, whereas the point symmetry has been broken in Fig. 5(b) and 5(c) owing to the initial nonzero vorticity (at time instant T=0.0) in the left spinning droplet, which leads to the liquid mass from the initial spinning droplet still have a large value of vorticity and thereby larger kinetic energy (KE) than the counterpart from the initial non-spinning droplet. The locally enhanced KE on one side of the ligament tends to elongate the united droplet to form a longer and thicker ligament, as shown in Fig. 5(c), and then breakup into satellite droplets. Furthermore, for another perspective, the variation of *B* and ω_0 can be interpreted as the variation of the spin angular momentum L_O for two droplets system and the spin angular momentum L_S for each droplet, as the coordinate axis shown in Fig. 5, which motivates to further study the influence of spinning direction, i.e. chirality, on the separation modes, that to be discussed in the following section.

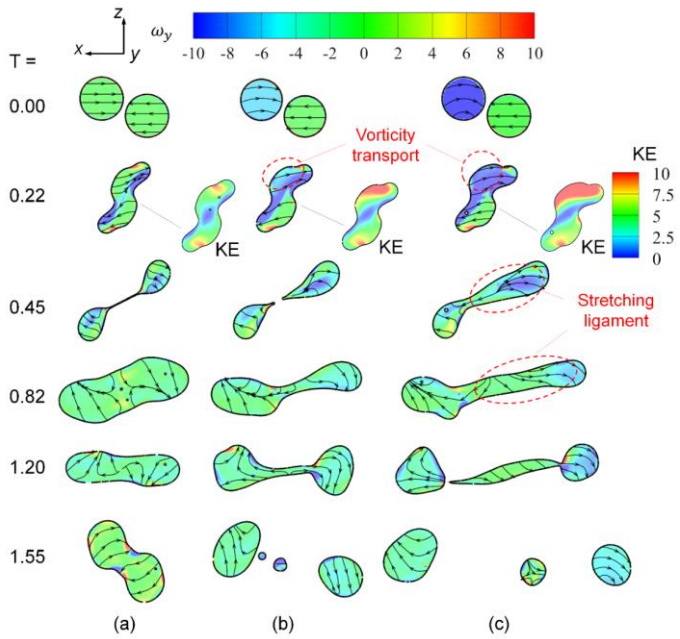

Figure 5. Contour of the vorticity and kinetic energy (KE) fields for the stretching separation mode at *B*=0.4 that shown in Fig. 4. (a) ω_0=0, (b) ω_0=3, and (c) ω_0=6.

IV. Influence of chirality on separation

Figure 6 compares the coalescence-separation boundary for collisions between droplets with different spin directions. For the stretching separation boundary, the droplet spin in Fig. 6(b) and 6(c) respectively enlarge and reduce the region of stretching separation by moving the boundary towards to small and large *B*. This is consistent with the above discussions in Fig. 5, that because L_O and L_S in Fig. 6(b) are in the same direction so as the stretching inertia is enhanced leading to the separation occurring at relatively small *B*. Similarly, L_O and L_S are in the opposite direction and a larger *B* are necessitated to separate the united droplet.

For the reflexive separation boundary at small *B*, the reflexive separation is suppressed by the droplet spin in Fig. 6(b), whereas is negligibly influenced by the droplet spin in Fig. 6(c), when compared to the boundary of the collision between two non-spinning droplets in Fig. 6(a). This can be understood as that, L_t in Fig. 7(a) and 7(c) is small so as the entire droplet deformation is approaching the nearly head-on collision by forming a long ligament followed by the reflexive separation. While for collisions in Fig. 7(b), droplet spin can lead to asymmetric vorticity

distribution on the round head of the ligament, as shown by the vorticity contour at T=0.75 and 0.94, and thereby suppress the ligament formation to separate into satellite droplets.

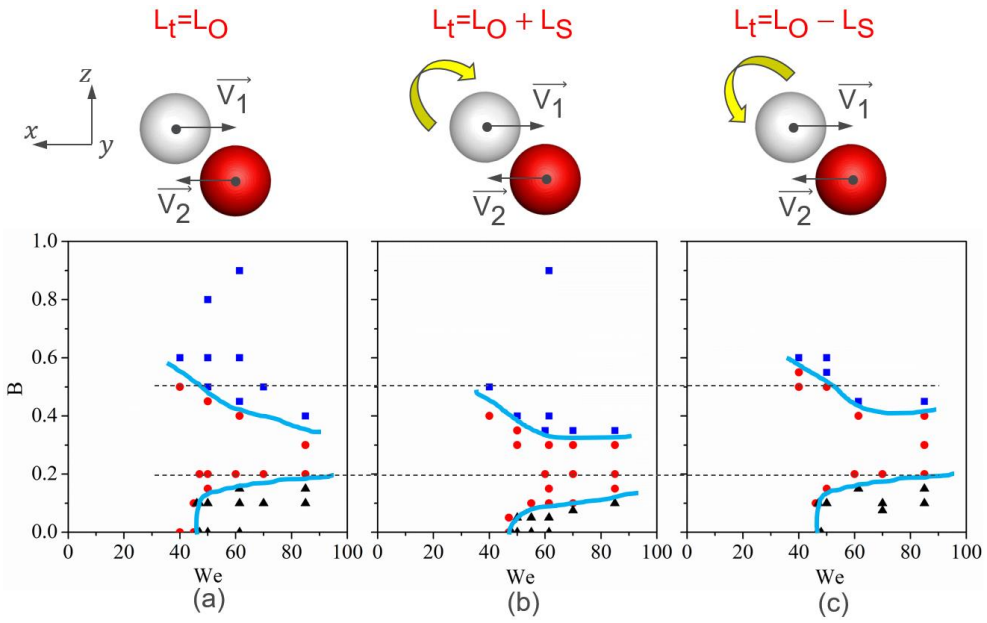

Figure 6. Influence of chirality of droplet spin on the variation of coalescence-separation transition boundary at B=0.15. (a) two non-spinning droplets, (b) $\boldsymbol{\omega_0}\hat{y}$=3, and (c) $\boldsymbol{\omega_0}\hat{y}$=-3.

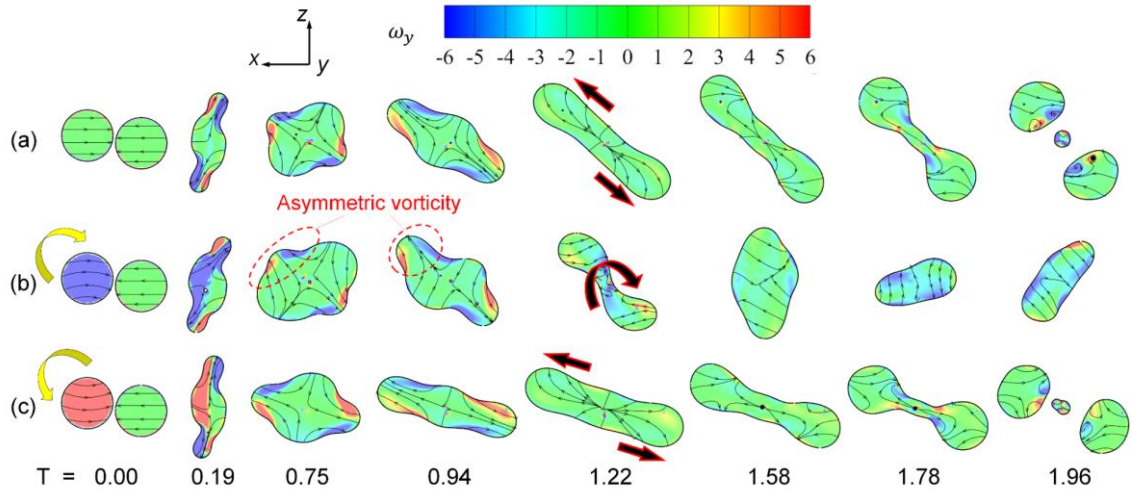

Figure 7. Contour of the vorticity field for the droplet separation at B=0.15 that shown in Fig. 6. (a) two non-spinning droplets, (b) $\boldsymbol{\omega_0}\hat{y}$=3, and (c) $\boldsymbol{\omega_0}\hat{y}$=-3.

Conclusions

A computational study on droplet separation that influenced by the initial droplet spinning motion was investigated based on a validated Volume-of-Fluid method. The results show that the droplet spin performs different mechanisms on the reflexive and stretching separations.

For the head-on collision, the reflexive separation tends to be suppressed by the droplet spin owing to the enhanced viscous dissipation. For nearly head-on collisions at small impact parameters, increasing the spin angular momentum of the merged droplet by an initial droplet spin would suppress the ligament formation and subsequent reflective separation; while decreasing the spin angular momentum of the merged droplet by a opposite droplet spin lead to approximately unchanged reflexive separation boundary to that of the collision between two

non-spinning droplets, because the spin angular momentum is approximately counteracted approaching the situation of the head-on collision. In addition, for collisions at large impact parameters, the increase or decrease of the spin angular momentum by the droplet spin can promote or suppress the stretching separation, respectively. The conclusion indicates that the local droplet deformation induced by the asymmetric droplet spin plays a significant role in affecting the droplet separation.

Acknowledgments
This work was supported by the China Postdoctoral Science Foundation (2020M680690), by Hong Kong RGC/GRF (through Grant No. PolyU 152188/20E) and by the Hong Kong Polytechnic University DGRF (through Grants No. G-UAHP).

Nomenclature
Non-dimensional and normalized variables

B	Impact parameter
L_t	Total angular momentum
L_O	Spin angular momentum for two droplets system
L_S	Spin angular momentum for each droplet
We	Translational Weber number
$\boldsymbol{\omega}$	Angular velocity vector / vorticity
$\hat{y}$	Component of the spin angular momentum in y-direction

References
[1]. M. Orme, 1997, Prog. Energy Combust. Sci. **23**(1), 65-79.
[2]. G. Brenn, 2011, N. Ashgriz, Editor. 2011, Springer, Berlin. p. 157-181.
[3]. N. Ashgriz and J. Poo, 1990, J. Fluid Mech. **221**, 183-204.
[4]. P. Brazier-Smith, S. Jennings, and J. Latham, 1972, *Proc. R. Soc. London, Ser. A*. **326**, 393
[5]. Y. Jiang, A. Umemura, and C. Law, 1992, J. Fluid Mech. **234**, 171-190.
[6]. A. Moreira, A. Moita, and M. Panao, 2010, Prog. Energy Combust. Sci. **36**(5), 554-580.
[7]. K.H. Al-Dirawi and A.E. Bayly, 2019, Phys. Fluids **31**(2), 027105.
[8]. J.-P. Estrade, H. Carentz, G. Lavergne, and Y. Biscos, 1999, Int. J. Heat Fluid Flow **20**(5), 486-491.
[9]. G. Finotello, J.T. Padding, N.G. Deen, A. Jongsma, F. Innings, and J. Kuipers, 2017, Phys. Fluids **29**(6), 067102.
[10]. J. Qian and C.K. Law, 1997, J. Fluid Mech. **331**, 59-80.
[11]. C. Rabe, J. Malet, and F. Feuillebois, 2010, Phys. Fluids **22**(4), 047101.
[12]. C. Tang, P. Zhang, and C.K. Law, 2012, Phys. Fluids **24**(2), 022101.
[13]. K.-L. Pan, K.-L. Huang, W.-T. Hsieh, and C.-R. Lu, 2019, Phys. Rev. Fluids **4**(12), 123602.
[14]. X. Chen and V. Yang, 2014, J. Comput. Phys. **269**, 22-39.
[15]. C. He, X. Xia, and P. Zhang, 2019, Phys. Fluids **31**(5), 052004.
[16]. C. He, X. Xia, and P. Zhang, 2020, Phys. Fluids **32**(3), 032004.
[17]. C. He and P. Zhang, 2020, Phys. Rev. Fluids **5**(11), 113601.
[18]. A. Munnannur and R.D. Reitz, 2009, Atom. Sprays **19**(7), 597-619.
[19]. S.L. Post and J. Abraham, 2002, Int. J. Multiph. Flow **28**(6), 997-1019.
[20]. S. Popinet, J. Comput. 2009, Phys. **228**(16), 5838-5866.
[21]. X. Chen, D. Ma, V. Yang, and S. Popinet, 2013, Atom. Sprays **23**(12), 1079-1101.
[22]. C. Tang, J. Zhao, P. Zhang, C.K. Law, and Z. Huang, 2016, J. Fluid Mech. **795**, 671-689.
[23]. X. Xia, C. He, D. Yu, J. Zhao, and P. Zhang, 2017, Phys. Rev. Fluids **2**(11), 113607.
[24]. X. Xia, C. He, and P. Zhang, 2019, PNAS **116**(47), 23467-23472.
[25]. P. Zhang and C.K. Law, 2011, Phys. Fluids **23**(4), 042102.